Recurrence Arrhythmias Quantification Analysis Using Simultaneous Optical and Electrical Cardiac Recordings

Mohammad Moualla[1], Jose Carlos Gomes Junior[1], Jimena Gabriela Siles Paredes[1], Tainan Cerqueira Neves[1], Vinicius de Paula Silva[1], Diogo C Soriano[1], Joao Salinet[1]

[1]Federal University of ABC, Sao Bernardo do Campo, Brazil

Abstract

Cardiac arrhythmias produce non-stationary signals that challenge classical frequency-domain analysis. Recurrence Quantification Analysis (RQA) characterises dynamical systems through the structure of their recurrence plots. We applied a unified RQA framework to optical and electrical recordings acquired simultaneously from seven isolated Langendorff-perfused rabbit hearts, with electrode-level pairing preserved. Sinus rhythm (SR), atrial tachycardia (AT), ventricular tachycardia (VT), monomorphic VT (MVT) and ventricular fibrillation (VF) were compared against the same-heart sinus baseline in a three-second window chosen by sensitivity analysis. Five RQA metrics were computed per electrode at a fixed 10 % recurrence rate and compared by within-heart paired Wilcoxon signed-rank tests. SR versus VF discrimination was strong and uniform across all hearts and both modalities. AT reproduced the same signature optically while the electrical response was largely absent. VT and MVT reversed between modalities, the electrical channel reporting greater local periodicity than SR and the optical less. The recurrence threshold increased in 19 of the 20 recording × modality combinations, the most consistent discriminator across the four arrhythmias.

1. Introduction

Sudden cardiac death from ventricular arrhythmia remains a principal cause of mortality worldwide, and the dynamical characterisation of these rhythms is a necessary condition for improved detection and ablation [1]. Classical analyses have relied mostly on frequency-domain decomposition or activation-time mapping, both of which assume a stationarity that is violated during ventricular fibrillation (VF) and ventricular tachycardia (VT) [2]. Nonlinear methods drawn from dynamical-systems theory do not depend on that assumption.

Recurrence Quantification Analysis (RQA) [3,4], characterises a dynamical system through the geometry of its recurrence plot, a binary matrix recording when the state of the system, reconstructed in a time-delay phase space, revisits a previous state to within a recurrence threshold (ε). It requires neither stationarity nor periodicity, applies to short windows, and produces interpretable scalar metrics summarising determinism, persistence and complexity. It has been applied to electrograms with promising results in arrhythmia classification [5].

Its application to simultaneous optical mapping, within a framework preserving electrode-level pairing across modalities, remains under-explored. Optical mapping with voltage-sensitive dyes [2,6] provides spatial information that electrograms cannot, each pixel averaging fluorescence over a small tissue. Most of the previous studies aimed to characterise cardiac signals undergoing fibrillation, so it is not established whether RQA could diverges from high frequency organised arrhythmias (atrial tachycardia (AT), VT, monomorphic VT (MVT)) from the sinus rhythm (SR). We therefore report a dual-modality RQA analysis of paired recordings from seven isolated Langendorff-perfused rabbit hearts, comparing SR with AT, VT, MVT and VF within the same animal.

2. Methods

2.1. Animal preparation

Seven New Zealand white rabbits were enrolled in the study. Animals were anaesthetised with buprenorphine followed by ketamine and xylazine and heparinised before sternal thoracotomy [7]. Hearts were excised, the aortic root cannulated, and the heart mounted on a Langendorff apparatus for retrograde perfusion at a constant pressure of 80 mmHg with modified Krebs–Henseleit buffer at 37 °C, oxygenated with 95% oxygen and 5% carbon dioxide. The Blebbistatin was added to the perfusate (21 µM bolus, 1.7 µM maintenance). Atrial arrhythmias were induced by burst pacing after carbachol (1 µM) infusion, ventricular arrhythmias by S1-S2 stimulation [7]. The hearts (H1–H7) were used for each comparison, between SR and the corresponding arrhythmia. Electrical signals were sampled at 4 kHz and optical signals recorded at 500 fps; every comparison used the same fixed 3-s analysis window. The distribution of hearts, regions, rhythms, and electrodes included in each comparison is summarised in Table 1.

Comparison	Hearts	Region	Recordings SR/Arrhythmia)	Electrodes (N)
SR vs AT	H6, H7	Atrium	2/2	32
SR vs VT	H3, H4, H5	Ventricle	3/3	48
SR vs MVT	H2, H3	Ventricle	2/2	32
SR vs VF	H1, H2, H3	Ventricle	3/3	48

Table 1. Experimental design and distribution of hearts, regions, rhythm comparisons, and matched electrodes included in the analysis.

2.2. Dual-modality recording and preprocessing

Each heart carried three platinum sixteen-electrode multi-electrode arrays (MEAs) in a four-by-four geometry, one per cardiac region (right atrium, left atrium and ventricle), acquired through an Intan 64-channel headstage and an Open Ephys acquisition board at 4 kHz. Panoramic optical mapping used three CMOS cameras at 120° intervals, the myocardium stained by Di-4-ANBDQPQ and recordings made at 500 FPS. The modalities were synchronised by a shared TTL trigger [8]. Electrical and optical signals preprocessing are summarized elsewhere [8]. Sixteen pixels per camera region were manually co-registered to the corresponding MEA electrode positions, establishing the pairing on which all cross-modal comparisons depend. Across the four comparisons this gives 160 paired positions in each modality, 320 in total. Residual offsets between modalities were resolved by per-region cross-correlation over ±50 ms.

2.3. Statistical analysis

A within-heart paired comparison for distinguishing SR and arrhythmia is performed: for each heart, modality and metric the paired difference Δ equal to (arrhythmia − SR) was computed at the sixteen matched positions. An electrode was included if its electrical SR DET reached 60%. Paired differences were tested against a null median of zero with a two-sided Wilcoxon signed-rank test [9] at $p < 0.05$, with effect size reported as Rosenthal's $r = |Z|/\sqrt{n}$ [10] and flagged as saturated when all sixteen electrodes share the sign of Δ. Electrodes within a heart share preparation, perfusion and dye loading and are not independent, so hearts are reported individually.

2.4. Recording selection and analysis window

The analysis window was fixed at 3 s throughout, following a sensitivity study across 1 s, 3 s and 5 s on all recordings. The window must hold enough cycles for diagonal structure to form while remaining short enough for the rhythm to be locally stationary [4]. Because Δ subtracts two recordings measured at the same window, any change common to both cancels; only the residual moves Δ. That residual was a median 3.2 % of the effect between 3 s and 5 s and 6.5 % between 1 s and 3 s.

2.5. Phase-space and RQA metrics

Each window was z-score normalised and embedded by Takens' time-delay reconstruction [11] with a fixed delay τ of 4 samples and embedding dimension m of 4, applied identically to every recording, electrode and modality. Fixing the embedding rather than deriving it per recording keeps the reconstructed phase spaces commensurable, which the paired difference between an arrhythmia and its own SR requires; the values were checked against the average mutual information [12] and false nearest neighbours [13] criteria. A Theiler window of round (1.5τ) excluded points close to the line of identity, and the recurrence plot was built by thresholding the pairwise Euclidean distance matrix at ε.

We adopted the fixed recurrence rate scheme. The threshold ε is not fixed in advance; it is set separately for each signal, to the tenth percentile of the pairwise distances lying outside the Theiler window, so that 10 % of state pairs are recurrent in every recording. Holding the recurrence quantity fixed makes the structural metrics comparable across rhythms [4]. The threshold thereby becomes signal-dependent: when the trajectory explores a larger phase-space volume, as during disorganised rhythms, ε must grow to maintain the same rate. For every recording and rhythm, the following metrics were computed at each electrode: determinism (DET), laminarity (LAM), trapping time (TT), entropy of diagonal-line lengths (ENT) and ε.

3. Results

3.1. Recurrence structure across the five rhythms

Figure 1 shows the recurrence plots of 3 s windows for all 5 rhythms in both channels. The spatial pattern of each recurrence matrix directly reflects the underlying electrophysiological mechanism and activation periodicity of the rhythm:

Sinus Rhythm (SR, CL ≈ 333 ms): Displays a broad, regular grid of interrupted diagonals parallel to the line of identity. Electrically, the wider spacing reflects the long baseline cycle length, while the optical channel reveals fine intra-beat action potential morphology.

Ventricular Tachycardia (VT, CL ≈ 200 ms): Maintains a highly periodic, moderately spaced diagonal grid. The reduced line spacing compared to SR reflects an accelerated local activation rate. Monomorphic VT (MVT, CL ≈ 143 ms): Generates dense, unbroken diagonal lines spanning the entire 3-second window in both channels. This uninterrupted trajectory highlights extreme temporal determinism and stationarity, consistent with a highly organized, rapidly circulating reentrant circuit. Atrial Tachycardia (AT, CL ≈ 107 ms): Produces extremely fine, tightly spaced diagonal stripes. The dense pattern corresponds to rapid, highly repetitive atrial activations induced by burst pacing. Ventricular Fibrillation (VF, mean activation interval ≈ 150–167 ms): Completely breaks the diagonal grid structure, leaving only short, fragmented segments and scattered single points. This disruption reflects turbulent phase-space dispersion,

wavebreak, and the loss of temporal self-similarity characteristic of chaotic fibrillatory conduction.

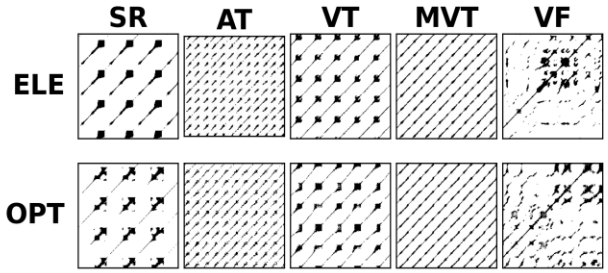

Figure 1. Binary recurrence plots of 3 s windows for the 5 rhythms in the electrical (ELE, top) and optical (OPT, bottom) channels.

3.2. Sinus rhythm versus atrial tachycardia

The shift from SR to AT represents a change from stable sinus activation to rapid, repetitive atrial depolarization. In optical signals, this change was consistent across all tested electrodes: DET decreased by 10.8–13.0 percentage points and LAM by 12.6–14.0 points, while ENT increased by 1.5–2.2 nats and ε by 0.65–0.80 (all p < 0.05, r ≈ 0.88). These changes indicate reduced temporal regularity and greater structural variation during AT, allowing optical measures to clearly separate the two rhythms. Electrical signals failed to show this pattern (only 4 of 10 tests significant, with inconsistent DET directions). This disparity likely stems from far- field interference and lower spatial resolution in electrical recordings, which blur localized activation and repolarization dynamics within the thin atrial myocardium.

3.3. Sinus rhythm versus VT and monomorphic VT

The shift from SR to ventricular tachycardia was associated with increased signal repetitiveness in electrical recordings. Both VT and MVT showed higher DET values than SR, increasing by 0.41–2.50 percentage points for VT and 0.56–7.21 points for MVT, along with an elevated recurrence threshold ε. This pattern reflects the regular, periodic depolarizations driven by ventricular reentrant circuits. In optical recordings, however, VT and MVT behaved differently. For VT, optical DET and LAM decreased relative to SR (DET falling by 0.96–4.83 percentage points), indicating lower temporal regularity. This cross-modal divergence suggests that while extracellular electrical signals remain periodic during VT, the optical signal captures localized action potential duration (APD) alternans and wavefront meandering. In contrast, MVT was the only rhythm where optical and electrical measures showed identical upward trends across DET, LAM and ε. This alignment reflects the highly organized, spatially stationary activation path characteristic of monomorphic reentry.

3.4. Sinus rhythm versus ventricular fibrillation

Unlike the atrial and ventricular tachycardia comparisons, both modalities showed changes in the same direction for VF: DET, LAM, TT, and ENT decreased, while ε increased, across all hearts and modality combinations, consistent with the loss of temporal organisation characteristic of a disorganised rhythm. All 30 tests (three hearts × two modalities × five metrics) reached significance, with correlation coefficients ranging from 0.67 to 0.88, although 24 tests were saturated. The magnitude of the change differed between modalities: optical ΔDET ranged from −11.69 to −9.27 percentage points, compared with −3.07 to −1.75 percentage points for the electrical signal.

Figure 2 presents all 4 comparisons as direction-of-effect heatmaps. Across the 20 recording × modality combinations ε increased in 19, the exception being one atrial heart electrically (−0.028, p = 0.756).

4. Discussion

This study reports a unified RQA analysis of optical and electrical recordings acquired simultaneously across 4 arrhythmias, with electrode-level pairing preserved throughout. Four principal findings emerge. First, SR-versus-VF discrimination is robust and uniform. All 5 metrics move in the same direction in all 3 hearts and both modalities, with most per-electrode tests saturated, and Figure 1 makes the structural contrast visible. Second, the optical modality produces larger effect sizes than the electrical in VF and AT, median |ΔDET| for SR-versus-VF being 9.94 against 2.82 percentage points, a ratio of 3.5. The relationship does not hold in MVT, where the electrical effect is larger.

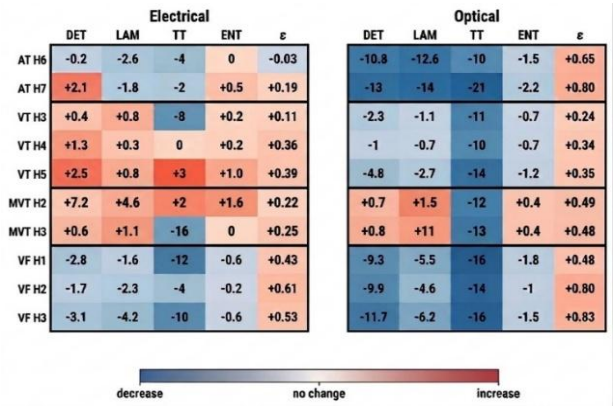

Figure 2. Direction-of-effect heatmaps for the 4 comparisons, one row per heart. Each cell gives the median Δ (arrhythmia − SR), with DET and LAM in percentage points, TT in milliseconds and ENT in nats.

Third, the AT, VT and MVT comparisons reveal a contrast not visible during VF: the optical modality reports VT as

less organised than SR while the electrical reports the reverse. This is resolved by what each modality physically measures. An electrode reads near-field activity from the patch of tissue beneath it, whereas an optical pixel averages fluorescence over a larger volume including the depth of the wall [6]. During organised reentry the wavefront circulates around a fixed circuit, so each electrode sees it arrive at the same site at regular intervals and the local electrogram is highly periodic beat-to-beat, whereas the sinus baseline carries the variability introduced by atrioventricular conduction. MVT, the most organised rhythm in the panel, is the only arrhythmia whose optical determinism metrics follow the electrical direction, suggesting the reversal tracks organisation rather than a fixed property of the optical channel.

Fourth, ε is the most robust cross-modality discriminator, increasing in 19 of the 20 recording × modality combinations. A rise in ε means the embedded trajectory covers a larger volume of phase space, so successive activations resemble one another less closely. ε also rises in MVT, the most regular rhythm recorded here, so it separates arrhythmia from sinus rhythm without measuring how disordered a rhythm is. Unlike the line-based metrics, ε is a percentile of the pairwise distance distribution and carries no upper bound imposed by the analysis window.

5. Conclusion

RQA is applied to simultaneous optical and electrical cardiac signals discriminates all 4 arrhythmias from the SR. Fibrillation disorganises both modalities alike, whereas the organised arrhythmias separate them, and the direction of that separation follows the degree of organisation of the rhythm. The adaptive recurrence threshold ε was the most consistent marker.

Acknowledgments

This study was supported by FAPESP 2018/25606-2, CNPq INCT INTERAS 409174/2024-6 and CAPES-GCUB; M Moualla by GCUB Call 001/2024 process 23006.008908/2025-73; J C Gomes Junior by CAPES 88887.986647/2024-00; J G Siles Paredes by FAPESP 2020/03601-9; T C Neves by FAPESP 2024/02521-2.

References

[1] G. A. Roth et al., “Global burden of cardiovascular diseases and risk factors, 1990–2019: update from the GBD 2019 study,” J. Am. Coll. Cardiol., vol. 76, no. 25, pp. 2982–3021, Dec. 2020.

[2] A. Schumacher, “Nonlinear organization of electrocardiogram and optical signals during ventricular fibrillation,” J. Electrocardiol., vol. 39, no. 4, pp. S146–S150, Oct. 2006.

[3] C. L. Webber Jr. and J. P. Zbilut, “Dynamical assessment of physiological systems and states using recurrence plot strategies,” J. Appl. Physiol., vol. 76, no. 2, pp. 965–973, Feb. 1994.

[4] N. Marwan, M. C. Romano, M. Thiel, and J. Kurths, “Recurrence plots for the analysis of complex systems,” Phys. Rep., vol. 438, no. 5–7, pp. 237–329, Jan. 2007.

[5] T. P. Almeida et al., “Characterization of human persistent atrial fibrillation electrograms using recurrence quantification analysis,” Chaos, vol. 28, no. 8, Aug. 2018, Art. no. 085710.

[6] I. R. Efimov, V. P. Nikolski, and G. Salama, “Optical imaging of the heart,” Circ. Res., vol. 94, no. 1, pp. 21–33, Jan. 2004.

[7] N. Zafalon Jr., J. W. M. Bassani, and R. A. Bassani, “Cholinergic-adrenergic antagonism in the induction of tachyarrhythmia by electrical stimulation in isolated rat atria,” J. Mol. Cell. Cardiol., vol. 37, no. 1, pp. 127–135, Jul. 2004.

[8] J. Siles et al., “An integrated platform for 2-D and 3-D optical and electrical mapping of arrhythmias in Langendorff-perfused rabbit hearts,” J. Physiol., 2025.

[9] F. Wilcoxon, “Individual comparisons by ranking methods,” Biometrics Bull., vol. 1, no. 6, pp. 80–83, Dec. 1945.

[10] R. Rosenthal, Meta-Analytic Procedures for Social Research. Newbury Park, CA, USA: Sage, 1991.

[11] F. Takens, “Detecting strange attractors in turbulence,” in Dynamical Systems and Turbulence, Warwick 1980, Lect. Notes Math., vol. 898. Berlin, Germany: Springer, 1981, pp. 366–381.

[12] A. M. Fraser and H. L. Swinney, “Independent coordinates for strange attractors from mutual information,” Phys. Rev. A, vol. 33, no. 2, pp. 1134–1140, Feb. 1986.

[13] M. B. Kennel, R. Brown, and H. D. I. Abarbanel, “Determining embedding dimension for phase-space reconstruction using a geometrical construction,” Phys. Rev. A, vol. 45, no. 6, pp. 3403–3411, Mar. 1992.

Address for correspondence:
Mohammad Moualla.
Federal University of ABC, Sao Bernardo do Campo, SP 09606-045, Brazil.
mohammad.moualla@ufabc.edu.b